An Improved Average Atomic Number Calculation for **Estimating Backscatter and Continuum Production in Compounds**

John Donovan^{1,*}, Andrew Ducharme², Joseph J. Schwab², Aurélien Moy³, Zack Gainsforth⁴, Benjamin Wade⁵, and Benjamin McMorran²

Abstract

It is often assumed that electron backscatter and continuum (bremsstrahlung) productions emitted from electron-solid interactions during X-ray microanalysis in compounds can be extrapolated from pure element observations by means of the assumption of average atomic number, or Z-bar (\bar{Z}) . For pure elements the average Z is equal to the atomic number, but this direct approach fails for compounds. The use of simple atomic fractions yields completely spurious results, and while the commonly used mass fraction Z averaging produces fairly reasonable results, we know from physical considerations that the mass of the neutron plays only a negligible role in such interactions below ~1 MeV. Therefore, including the mass or atomic weight in such calculations can only introduce further errors in these models. We present an expression utilizing atomic fractions of the atomic numbers of the elements in the compound (Z fraction), with an exponent to account for the variation in nuclear screening as a function of the element Z value.

Key words: average atomic number, backscatter, compounds, continuum, EPMA, z-bar

Introduction

Electron probe microanalysis (EPMA) is a powerful analytical technique for characterizing the composition of a material by identifying and quantifying peaks in the X-ray spectra caused by the ejection and refilling of orbital electrons of atoms within the material. Yet to properly interpret these results, researchers must also model the modification of the spectra due to electron scattering off atomic nuclei. Electron-nucleus scattering affects the spectra in two ways: backscattered electrons (BSE) modify the relative strengths of characteristic X-ray peaks while Bremsstrahlung, or "braking" radiation, forms a continuous background signal in the X-ray spectra called the continuum.

Such scattering models combine known information about pure elements for estimating backscatter and continuum productions in compounds. Currently, microanalysis researchers generally use the average mass fraction of elements in a material to model average Z in compounds, however, this approach is flawed. The mass fraction differentiates between elements in a compound by atomic weight, the average mass of the elemental isotopes scaled by their terrestrial abundance. Atomic weight does not scale linearly with the atomic number of protons, as it includes neutrons as well. At the typical beam energies used in EPMA, electrons do not scatter from neutrons, only charged particles, and so atomic weight is an incorrect quantity to use in our models.

It is true the mass of the nucleus can affect electron scattering when the incident electron transfers enough energy for the nucleus to have a non-negligible recoil. However, this requires an accelerating voltage far higher than in EPMA operating conditions. Consider an elastic collision of an electron and a nucleus at rest. The maximum energy transfer to the nucleus occurs with a scattering angle of 180°. The recoiling nucleus of mass M acquires increased kinetic energy ΔE

$$\Delta E = 2M \frac{m_e^2}{(m_e + M)^2} v^2$$
 (1)

where m_e is the mass of the electron and ν is the initial velocity of the electron. Since m_e is much smaller than M, $m_e + M$ equals M to a very good approximation, and we can express ΔE as

$$\Delta E \approx 4 \frac{m_e}{M} E \tag{2}$$

where *E* is the initial kinetic energy of the electron. The largest energy loss occurs in hydrogen, where $4m_e/M \sim 4/2000$. Hence, in each purely elastic collision, an electron loses a maximum of $\sim 0.2\%$ of its kinetic energy to the nucleus. For the vast majority of collisions, with much smaller scattering angles, the energy loss is considerably less than this. For heavier nuclei, such as iron, it is smaller still (by a factor of A, the atomic weight of the nucleus). The difference in this quantity, for two isotopes of the same element, is even smaller yet: for ³⁶Fe and ³⁷Fe, the difference in fractional energy loss per nuclear collision is, at most, 6.10^{-8} . Earlier studies have

¹CAMCOR, University of Oregon, 1443 East 13th Ave., Eugene, OR 97403, USA

²Department of Physics, University of Oregon, 1371 East 13th Ave., Eugene, OR 97403, USA

³Geoscience Department, University of Wisconsin-Madison, 1215 W Dayton St, Madison, WI 53706, USA

⁴Space Sciences Laboratory, Univ. of California at Berkeley, 7 Gauss Way, Berkeley, CA 94720, USA

⁵Adelaide Microscopy, The University of Adelaide, NG13, Frome Road, Adelaide, SA 5005, Australia

^{*}Corresponding author: John Donovan, E-mail: donovan@uoregon.edu

demonstrated the insignificance of mass to modeling both electron backscattering and continuum production in solids by empirical comparisons of stable isotope pairs of elements (Donovan & Pingitore, 2002; Donovan et al., 2003). Mass fraction has historically been the most accurate model, but some other form of atomic fraction averaging must be utilized for improved calculations of average Z in compounds.

Atomic Number Averaging

Although various alternative average atomic number, or Z-bar, expressions utilizing atomic number fractions are found in the scientific literature for both backscatter and continuum productions (Joyet et al., 1953; Danguy & Quivy, 1956; Everhart, 1960; Büchner, 1973; Herrmann & Reimer, 1984; Howell et al., 1998), simple mass fraction averaging is traditionally utilized by microanalysts (Goldstein et al., 1992):

$$\bar{Z}_{(c_i)} = \sum_{i=1}^n c_i Z_i$$
 (3)

where $\bar{Z}_{(c_i)}$ is the mass fraction average Z or Z-bar, c_i is the conventional mass fraction of element i, and Z_i is the atomic number of element i present in the compound.

However, from the first principle physics considered above (Equations (1) and (2)) we know that mass has essentially no effect on these productions. Most serendipitously, it is only due to the fact that A/Z is roughly a constant over the periodic table (where A is the atomic weight), that this assumption of mass fraction averaging for compounds is a useful approximation at all. In fact, the error due to the inclusion of atomic mass in atomic number average calculations depends on the specific A/Z ratios of the elements in that compound. If the elements all share similar A/Z ratios, the error is small, but if the elements in the compound have relatively disparate A/Z ratios, the introduced error due to mass averaging can exceed 30%, as will be discussed.

Given that atomic mass is essentially irrelevant to determining composition by X-ray microanalysis where the electron beam energy is significantly less than 1 MeV, a model based on atomic number is more suitable. Our approach is to modify

the mass fraction average \bar{Z} as shown in equation (3), by defining an alternative fractional method, the Z Fraction, as follows:

$$\bar{Z}_{(z_i)} = \sum_{i=1}^{n} z_i Z_i \tag{4}$$

where Z_i is again the atomic number for element i, and the Z fraction z_i is defined as:

$$z_i = \frac{a_i Z_i}{\sum_{j=1}^n a_j Z_j} \tag{5}$$

and a_i is the atomic fraction for element i. This expression is algebraically equivalent to the expression from Saldick & Allen (1954). However, to account for screening, we raise the Z fraction to an exponent x generally less than 1:

$$\bar{Z}_{(z_i^{(x)})} = \sum_{i=1}^n z_i^{(x)} Z_i \tag{6}$$

where $z_i^{(x)}$ is the modified Z fraction defined by:

$$z_i^{(x)} = \frac{a_i Z_i^x}{\sum_{i=1}^n a_i Z_i^x} \ . \tag{7}$$

Based on empirical backscatter and continuum measurements we obtain an approximate best fit to Eqs. (6) and (7) for x of around 0.7 to 0.8. The exact value of this exponent depends on the specific shape and density of the compound charge distribution.

Results

Empirical measurements of backscatter and continuum productions were performed on the Cameca SX100 at the University of Oregon and the Cameca SXFive at the University of Adelaide using the Probe for EPMA v13.1.7 software on both instruments. Monte Carlo modeling was performed at the University of Oregon and University of Wisconsin using the PENEPMA 2012 software (Llovet & Salvat, 2017).

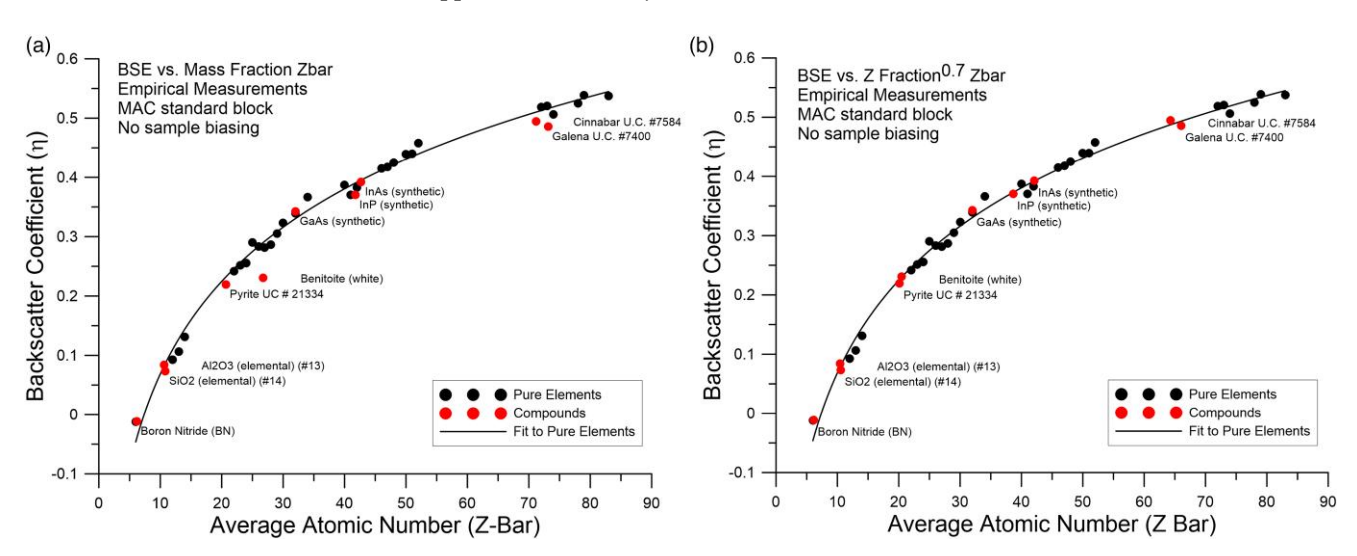


Fig. 1. Measurements of electron backscatter on standard samples by measuring the ratio of the absorbed and Faraday cup currents, i.e., $\eta = 1 - \frac{i_{absorbed}}{i_{landay}}$, for (a) mass fraction average Z, and (b) Z fraction average Z using an exponent of 0.7. This backscatter coefficient measurement is not absolutely accurate due to re-absorption of secondary electrons, but suffices for a relative comparison. Note benitoite (BaTiSi₃O₉), cinnabar (HgS) and galena (PbS) are compounds containing elements with significantly different A/Z ratios.

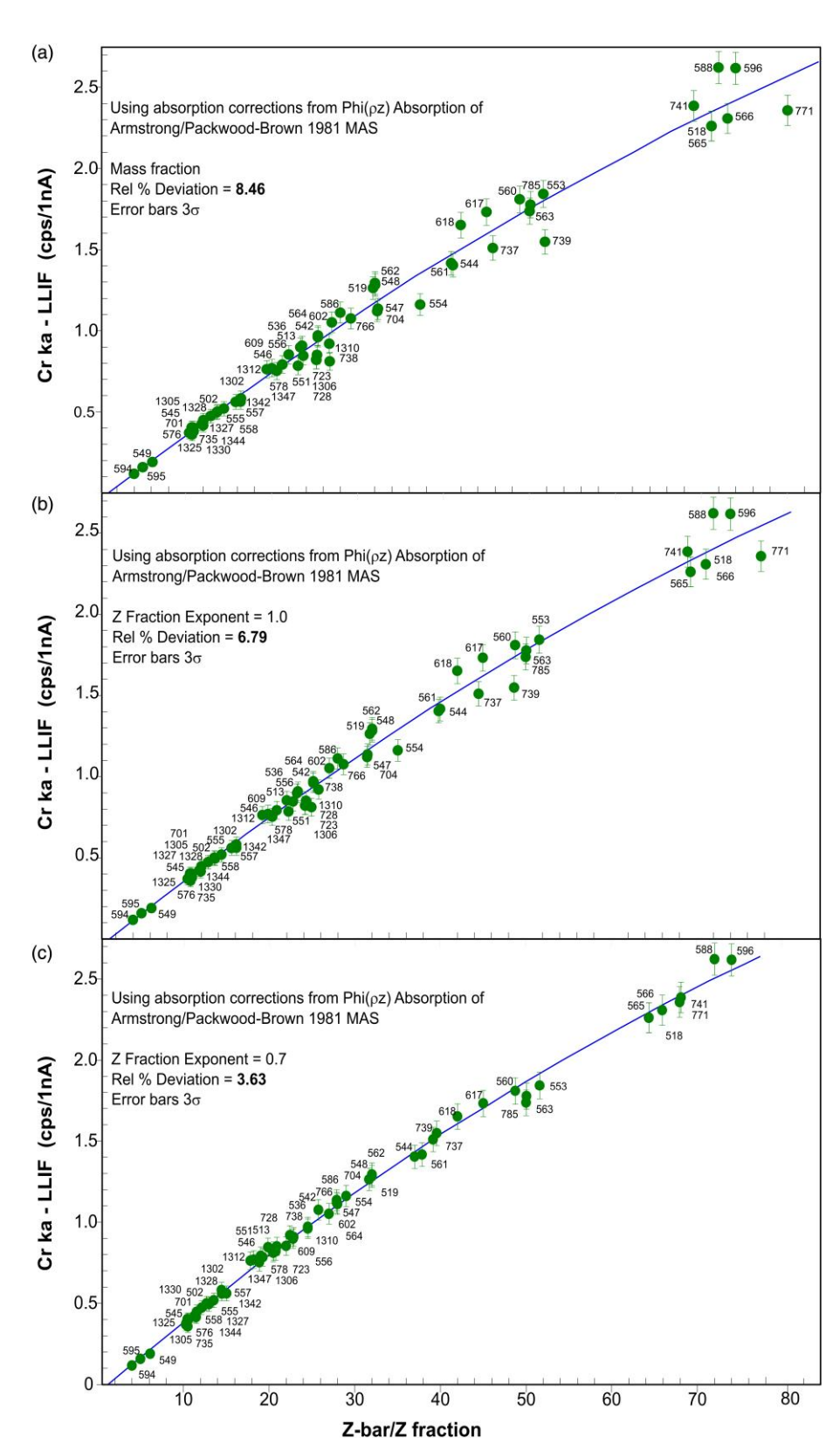


Fig. 2. Measurements of continuum intensity (absorption corrected) using a 15 keV electron beam energy at the chromium Kα emission energy position for pure elements and compounds that do not contain Cr, plotted using (**a**) mass fraction average Z, (**b**) Z fraction average Z with exponent 0.7. The blue line is the best fit to the data using a 2nd order polynomial.

First we examine empirical measurements of absorbed and faraday cup beam currents as seen in Figure 1, where the pure elements are plotted as black symbols and selected standard compounds of known composition are plotted as red

symbols for mass fraction average Z in (a), and modified Z fraction in (b). Compounds containing elements with a variety of A/Z ratios show improved correlation using the Z fraction expression with an exponent of 0.7.

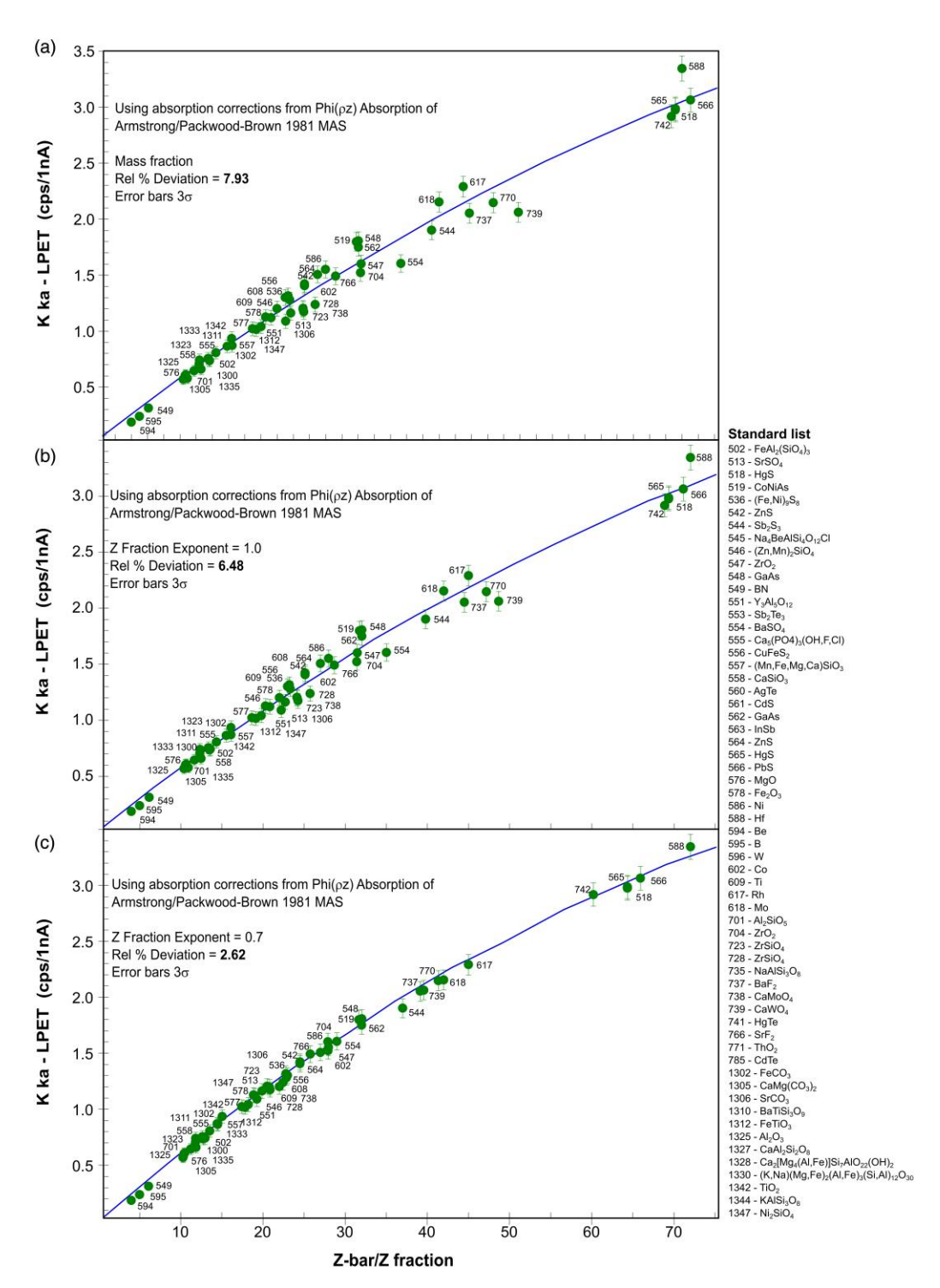


Fig. 3. Measurements of continuum intensity (absorption corrected) using a 15 keV electron beam energy at the potassium $K\alpha$ emission energy position for pure elements and compounds that do not contain K, plotted using (**a**) mass fraction average Z, (**b**) Z fraction average \bar{Z} with exponent 1.0, and (**c**) Z fraction average \bar{Z} with exponent 0.7. The blue line is the best fit to the data using a 2nd order polynomial.

In Figures 2 and 3, and 4 we show results from high precision continuum X-ray empirical measurements for a range of pure elements and standard compounds for continuum energies at the Cr K α , K K α , and Na K α emission line energies, respectively, for compounds that do not contain those elements. All continuum intensities were corrected for absorption using the method of Packwood & Brown (1981), though any absorption correction will produce similar results. In these three figures we show (a) for mass fraction, (b) Z fraction (exponent = 1.0), and

(c) Z fraction (exponent = 0.7) that the best correlation is seen for the Z Fraction average Z method with an exponent of 0.7.

Subsequently we performed a number of Monte Carlo simulations for both backscatter and continuum productions. In Figure 5, we plot the calculated backscatter fraction from high precision Monte Carlo modeling in PENEPMA 2012, for both pure elements and selected compounds, which include compounds containing elements with a variety of A/Z ratios. The pure elements from atomic number 10 to atomic

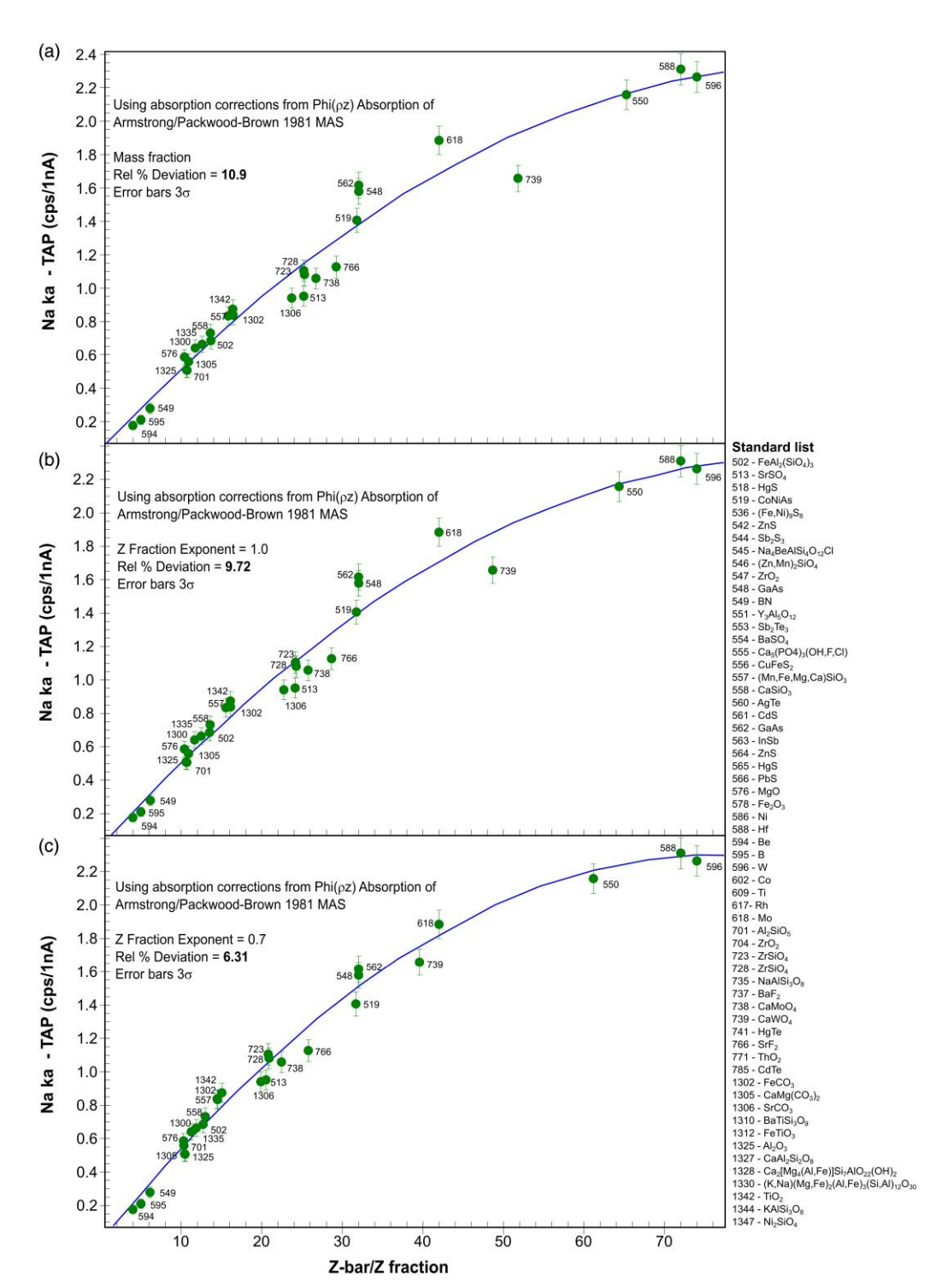


Fig. 4. Measurements of continuum intensity (absorption corrected) using a 15 keV electron beam energy at the sodium $K\alpha$ emission energy position for a number of pure elements and compounds that do not contain Na, plotted using (a) mass fraction average Z, (b) Z fraction average Z with exponent 1.0, and (c) Z fraction average Z with exponent 0.7. The blue line is the best fit to the data using a 2nd order polynomial.

number 85 are plotted as a line, and the compounds are plotted as symbols, where we have assumed mass fractional averaging for the calculation of average Z in the compounds in (a) and using the modified Z fraction with an x exponent of 0.7 for (b), obtained from the best fit empirical data from Figure 1.

Figure 6 shows results from PENEPMA Monte Carlo modeling of generated continuum intensities at 2 and 8 keV for pure elements and a number of compounds using both mass fraction averaging and modified Z fraction averaging with x = 0.7. We

note results from these figures suggest a possible small energy dependence on the exact value of the exponent for these productions as discussed by Moy et al. (2021). Experimental and theoretical investigations of this subtle interdependency are ongoing.

In summary, both experimental measurements and theoretical calculations clearly show that the backscattered coefficients and the continuum intensities are best modeled using a Z fraction model with an exponent of approximately 0.7, which we designate the "Yukawa Z fraction."

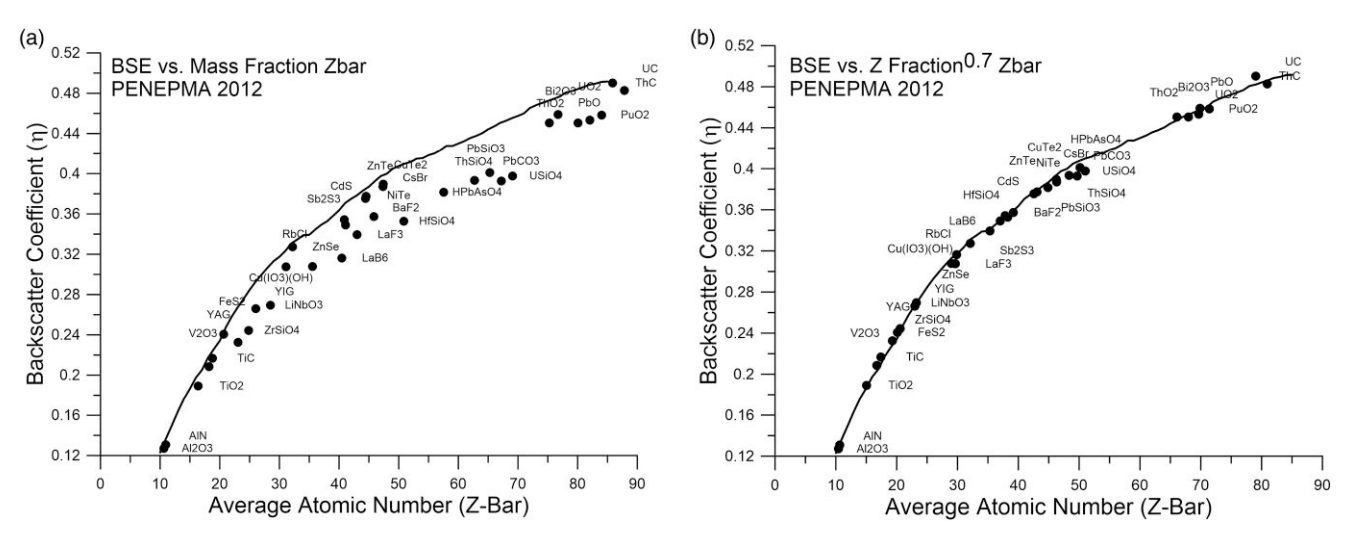


Fig. 5. Monte Carlo calculations from PENEPMA 2012 of the electron backscatter coefficient from pure elements plotted as a line, and compounds plotted as symbols, for (a) mass fraction average Z, and (b) Z fraction average Z using an exponent of 0.7.

The Yukawa Potential and Its Expected Accuracy

Here we review and discuss a simplified model of electron-atom scattering to estimate a theoretical value of the Z fraction exponent $x = \sim 2/3$. We use the Yukawa potential V(r) (Yukawa, 1935), also called a screened Coulomb or Wentzel potential, to describe the interaction of the incident electron and the target atom. Mathematically,

$$V(r) = CZ \frac{e^{-r/R}}{r}$$

where r is the radial distance from the atom nucleus, R is the screening length, and $C = -\frac{e^2}{4\pi\epsilon_0}$ is a constant. The screening length $R = a_0 Z^{-1/3}$ is given by the Thomas-Fermi model (Kittel, 2004; Carron, 2006; Egerton, 2011), where a_0 is the Bohr radius.

The Yukawa potential has been used successfully for many processes in physics dating back to Yukawa's original efforts to describe interactions between nucleons (Yukawa, 1935). It is commonly used to model a Coulomb potential screened by another charge distribution, such as the potential of atomic nuclei surrounded by electrons (Kittel, 2004). Despite its advantages and pedigree, the Yukawa potential does not describe the actual charge distribution exactly. It suffers from infinite charge density at the origin, just as does the Coulomb potential, and it does not model the intricate structure of overlapping electron orbitals described by a fully relativistic quantum mechanical model. We use density functional theory (DFT) to accurately describe real charge distributions and test if the Yukawa potential is an appropriate model for our purposes.

Using the atomic (ld1.x) package contained in the Quantum Espresso software (Giannozzi et al., 2009, 2017), we calculated the radial charge distribution for hydrogen, oxygen, and calcium atoms as a function of shell. We used the Perdew-Burke-Enzerhof exchange correlation functional (Perdew et al., 1996). In Figure 7, we plot the radial charge distribution $4\pi r^2 \rho(r)$ computed for hydrogen and oxygen. In (a), the radial charge distribution in hydrogen indicates a maximum 1 Bohr (a.u.) interaction range for the electron. In (b),

we show the radial charge distribution of the 1s, 2s, and 2p orbitals in oxygen. Each orbital dominates a specific radial distance from the nucleus. The 1s orbital is pulled in to about 0.2 Bohr while the 2s and 2p orbitals peak at about 0.8 Bohr.

In Figure 8, we explore the radial charge distribution in the larger and more complex calcium atom. Figures 8a and b show the radial charge distribution to emphasize the interaction ranges of each orbital. Again, particular shells dominate different radial ranges: the n = 1 shell dominates r < 0.1 Bohr, n=2 dominates 0.1 < r < 0.6 Bohr, and n=3 dominates r > 0.6 Bohr. In Figure 9, we plot the DFT-based V(r) distributions for each element alongside an arbitrary Yukawa potential chosen to best fit V(r) outside 1 Bohr. Despite the multi-lobed quantum mechanical nature of the charge density, the corresponding electric potential V(r) yields a fairly traditional looking distribution for H, O, and Ca. Thus, the Yukawa potential is correctly fitting the medium- to longrange regimes of the potential. We conclude that the Yukawa potential is a useful approximation of the atomic potential and a suitable model for electron microprobe work. The use of a more accurate charge distribution (such as Mott scattering) would improve the modeling primarily for light multi-electron atoms such as O.

The Differential Scattering Cross Section of the Yukawa Potential

We will now describe electron-atom scattering by deriving the angular differential cross section $d\sigma/d\Omega$ of the Yukawa potential in the first Born approximation. This calculation can be found in many standard microscopy and quantum mechanics textbooks (Reimer, 1998; Griffiths & Schroeter, 2020). Specifically, $d\sigma/d\Omega$ is proportional to the probability of the incident electron scattering from the spherically symmetric atom into a differential solid angle $d\Omega$.

Quantum scattering theory assumes that an incident plane wave, after interacting with a potential, propagates as a spherical wave with angular dependence described by the complex scattering amplitude $f(\theta)$. The first Born approximation is a standard technique to solve the time-independent Schrödinger equation for the scattering amplitude and consequently the

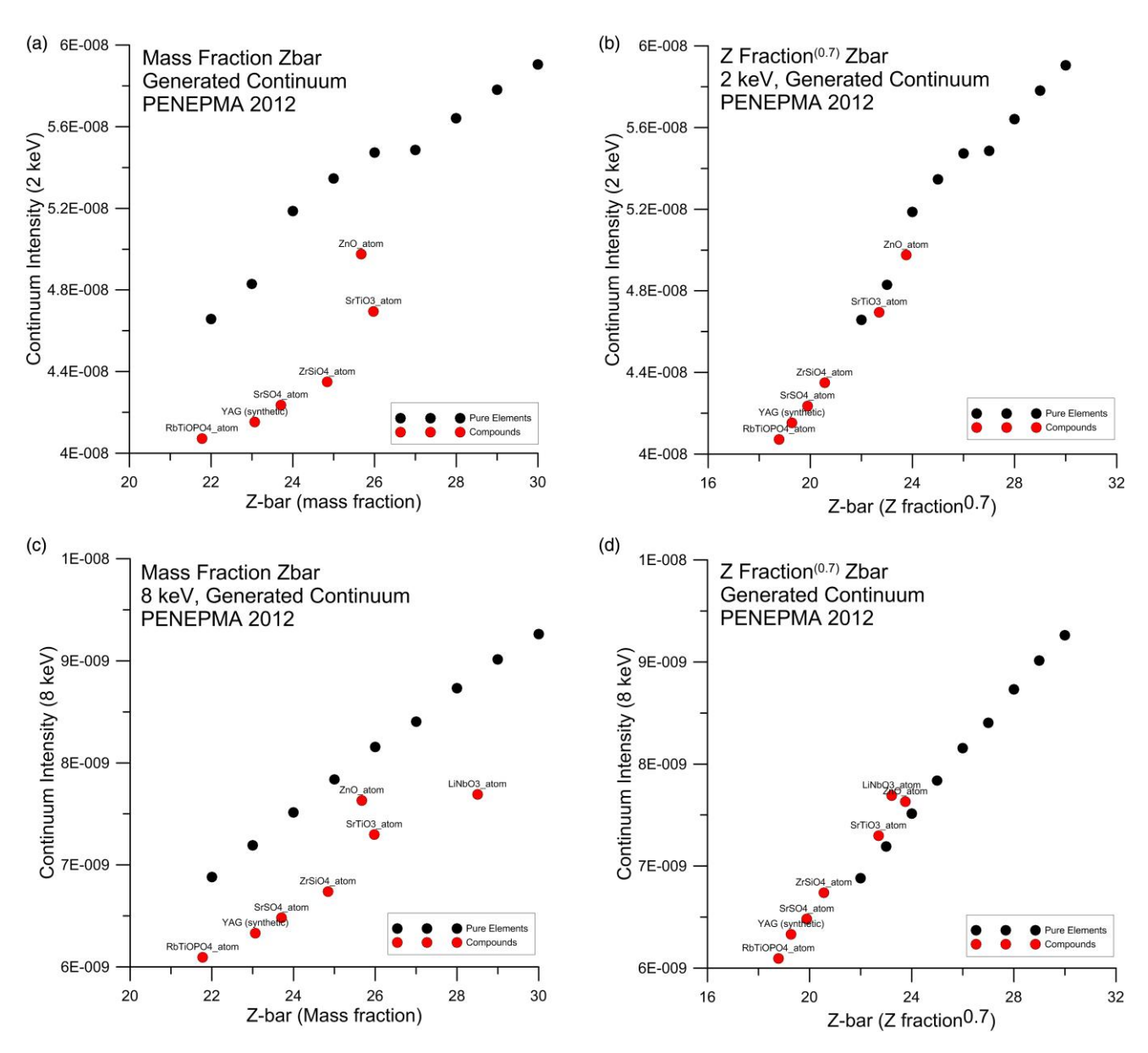


Fig. 6. PENEPMA 2012 Monte Carlo (generated) continuum intensity simulations for pure elements from titanium to zinc (black symbols) and a number of compounds (red symbols) containing elements with relatively disparate A/Z ratios, for (a) mass fraction average Z at 2 keV, (b) Z fraction average \bar{Z} with exponent 0.7 at 2 keV, (c) mass fraction average Z at 8 keV, and (d) Z fraction average \bar{Z} at 8 keV. The y axes values are in probability density units, i.e., $1/(eV^*sr^*electron)$.

differential cross section $\frac{d\sigma}{d\Omega} = |f(\theta)|^2$. This approximation is valid for accelerating voltages above 1 keV and should be easily satisfied in electron probe microanalysis.

For a projectile of mass m scattering from a spherically symmetric potential U(r), the scattering amplitude is,

$$f(\theta) = -\frac{2m}{\hbar^{2}\kappa} \int_{0}^{\infty} rU(r)sin(\kappa r) \ dr,$$

where $\kappa = 2ksin(\theta/2)$ includes the relativistic momentum of the incident electron via $\hbar k = \gamma mv$. Now for the Yukawa potential,

$$f(\theta) \propto \frac{1}{\kappa} \int_{0}^{\infty} e^{-\frac{r}{R}} sin(\kappa r) dr = \frac{1}{\left(\frac{1}{R}\right)^{2} + \kappa^{2}}.$$

Thus, we have our differential cross section

$$\frac{d\sigma}{d\Omega} = |f(\theta)|^2 = \frac{4\gamma^2 Z^2}{a_0^2} \left[\frac{1}{\left(\frac{1}{R}\right)^2 + 4k^2 sin^2\left(\frac{\theta}{2}\right)} \right]^2.$$

Rearranging, and inserting the Thomas-Fermi screening length *R* above,

$$\frac{d\sigma}{d\Omega}(\theta) = 4a_0^2 \gamma^2 Z^{2/3} \left[1 + (2ka_0 Z^{-1/3})^2 \sin^2\left(\frac{\theta}{2}\right) \right]^{-2},$$

we can see the cross section, when evaluated at $\theta = 0$, is proportional to $Z^{2/3}$.

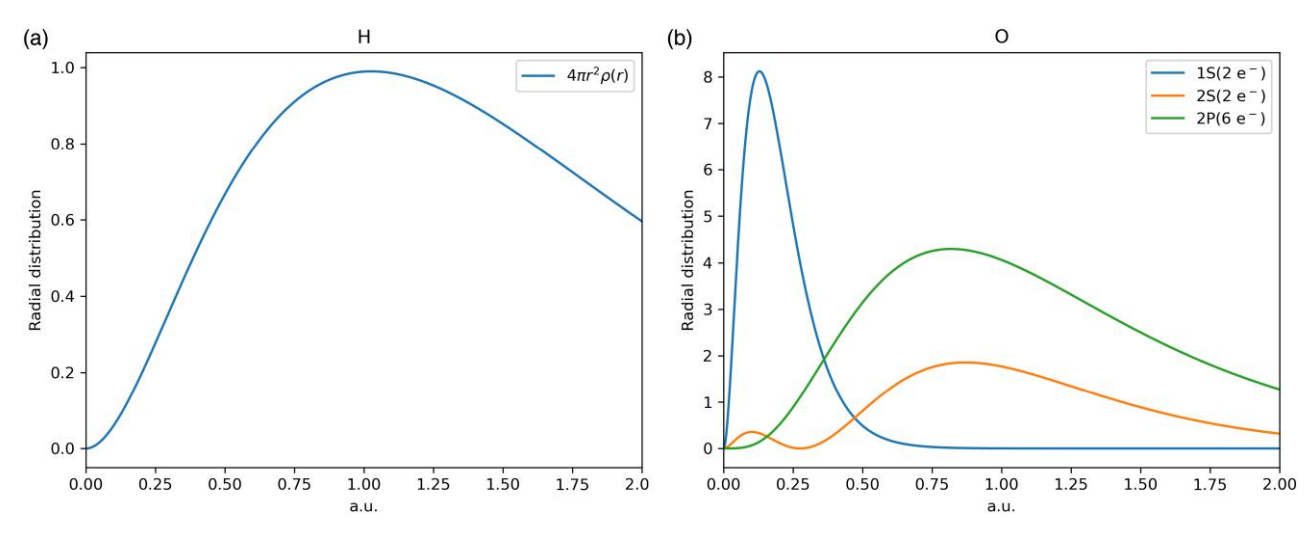


Fig. 7. The radial charge distributions $4\pi r^2 \rho(r)$ of orbitals for hydrogen and oxygen atoms: (a) the H atom (which is only due to the 1s electron) and (b) individual orbitals in O (not all orbitals are fully occupied).

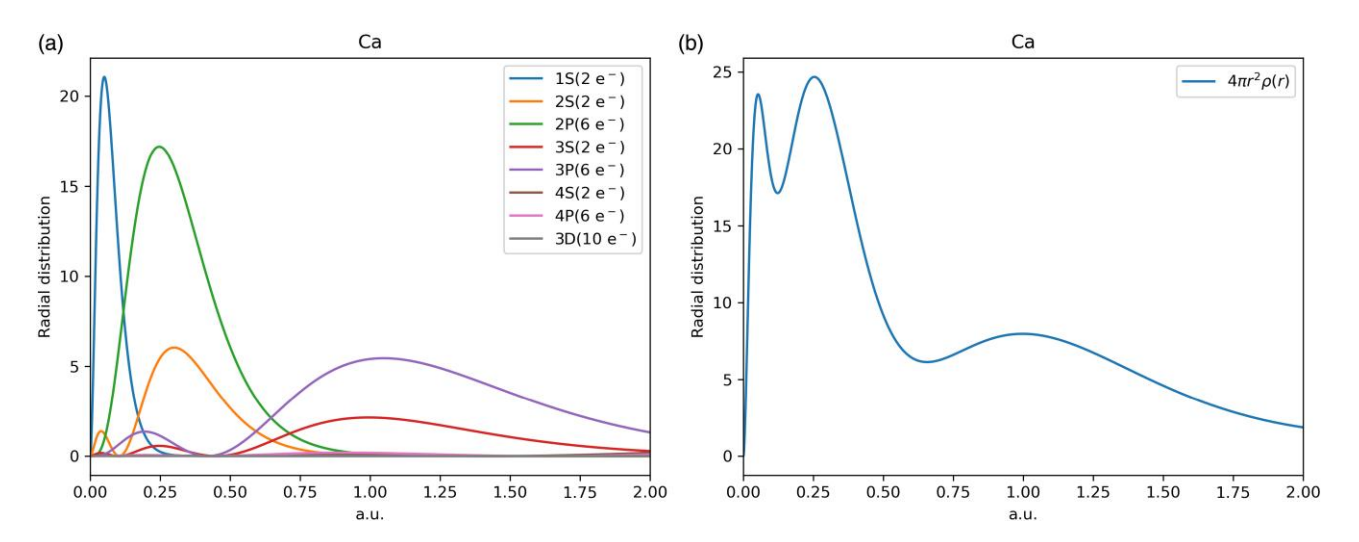


Fig. 8. Plots showing the charge distribution $4\pi r^2 \rho(r)$ of electrons in the calcium atom (a) for each orbital individually (not all orbitals are occupied), and (b) for all occupied Ca orbitals combined.

The Modified Z Fraction Exponent

Here we argue that both continuum and BSE emissions are most heavily dominated by forward scattering, and so both signals scale roughly with $Z^{2/3}$ according to the simple model derived above. In Figure 10a, we plot the differential cross section, an expression for scattering angle probability, versus scattering angle and atomic number for an accelerating voltage of 20 keV. The key qualitative feature of this scattering distribution is its sharp peak at low scattering angles and the maxima at $\theta = 0$ for all Z values. In fact, with increased accelerating voltages this peak at small θ is only accentuated. Note the black line which highlights the $Z^{2/3}$ trend at small θ . We further isolate particular atomic differential cross sections, again at 20 keV, in Figure 10b. At both ends of the periodic table, an atomic nucleus barely deflects almost all the electrons it interacts with. For Z = 5, 95% of all electrons are scattered within 9 degrees of their initial trajectory, while for Z = 96, 95% of all electrons are scattered within 15 degrees of their initial trajectory.

We also utilized PENELOPE 2012 (Llovet & Salvat, 2017) Monte Carlo simulations to substantiate this theoretical model. These simulations were performed with 100,000 total electrons incident on aluminum (Z = 13), copper (Z = 29), and gold (Z = 79) at 15 keV. We examined all electrons which made it back out of the sample with an energy greater than 500 eV. We next computed the average scattering angle for each electron, and took the mean of these averages for all backscattered electrons. We then found the same mean after discarding the largest scattering event for each backscattered electron. These are the Average Scattering Angle and Average Small Angle Scattering, respectively, in Table 1. We find, after removing the maximum scattering angle, this reduced mean is significantly smaller than the simple mean and well within the realm of small angle scattering for all three elements.

These simulations tell us that the vast majority of electrons essentially continue in the direction of their original momentum when incident on any atom in the sample as shown in Figure 11. However, most BSEs are electrons that undergo

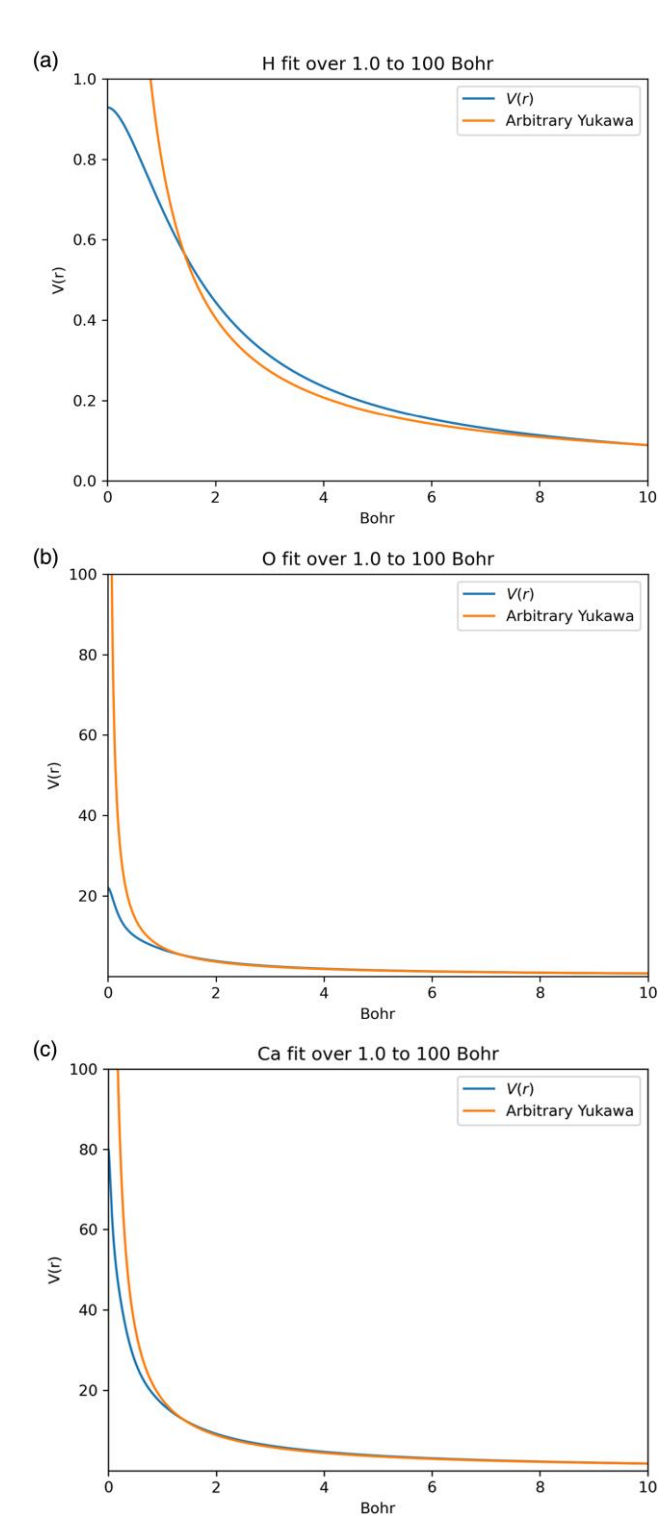


Fig. 9. The electric potentials V(r), calculated from charge distributions derived from DFT, plotted against a Yukawa function least squares fit to V(r) over radial distances from 1 to 100 Bohr radii plotted from 0 to 10 Bohr. See (a) for H atom, (b) for O atom, and (c) for Ca atom.

one or two rare higher-angle scattering events at the beginning of their history inside a material. These high-angle scattering events turn the BSE's trajectory back in the direction of the surface. These BSEs then experience many more scattering events as they travelled back towards the surface. As established above, the likelihood of low-angle scattering events dominate, and this probability converges towards $Z^{2/3}$. Of

course, the electron could also undergo a second, third, or nth higher-angle reorientation, but these more unlikely sequences yield an electron which stays within the sample unmeasured. Thus, the overall probability for an electron to re-emerge from the surface, becoming a backscattered electron, is proportional to the probability of the dominant lowangle scattering events.

Electron scattering events also produce X-ray radiation as these redirections of the electron trajectory necessitate the deceleration that gives bremsstrahlung its name. We measure the aggregate of these signals as continuum X-rays, which are generated predominantly at the low energy limit as shown in Figure 12. For increasing energy in continuum production, the decreased probability of scattering events large enough in angle, hence energy, limits the continuum production until reaching zero at the Duane-Hunt limit. Thus, it can reasonably be claimed that continuum X-rays are predominantly generated by electrons scattering at low angles, since this process is the overwhelmingly dominant one. Thus, the Z-proportionality of X-ray continuum also scales approximately as $Z^{2/3}$.

We do observe variation in the Z exponent from $Z^{2/3}$ predominantly towards Z^2 in empirical measurements of BSE and continuum emissions of compounds. Figure 13 shows experimental evidence of differing best fit Z Fraction exponents from empirical continuum measurements over a range of emission energies. This is further corroborated from PENEPMA 2012 (Llovet & Salvat, 2017) Monte Carlo simulations of the optimized Z fraction exponents for pure elements and compounds as shown in Figure 14. We would predict, in general, deviations from our model to manifest as a slight increase in the Z exponent. When fitting the differential cross section to Z^x while treating a nonzero θ as a parameter, the exponent x rises monotonically with θ to a bound of x = 2. Figure 15 depicts this transition and the details of the calculations are shown in the Appendix.

Implications for Microanalysis

Considerations from physics, empirical measurements, and Monte Carlo modeling all demonstrate that mass has essentially no effect on the generation and emission of backscattered electrons and continuum X-rays in electron-solid interactions at typical electron energies utilized in electron probe microanalysis.

But what about the main focus of microanalysis: the generation and emission of characteristic X-rays for elemental quantification? We do not at this time attempt to provide a Yukawa Z fraction based model for the treatment of characteristic emissions, however we can say that such a model would be entirely consistent from what we already know from physics, which is that both wavelength and energy dispersive X-ray spectrometries (WDS and EDS) do not weigh atoms. They count them!

Simply put, the use of mass fractions in the physics of electron probe microanalysis induces a bias equal to the relative differences in the A/Z ratios of the elements involved. For some elements this difference in A/Z is small, but for other compounds these A/Z differences can become quite large. For example, the relative difference in mass fraction versus the Yukawa Z fraction for average Z in MgO for Mg and O is under 1%, while for a compound such as PbS, the differences in A/Z yield average Z values that vary by more than 20% relative (Donovan et al., 2003) as shown in Table 2. If we estimate the backscatter correction in PbS to be ~20% of the

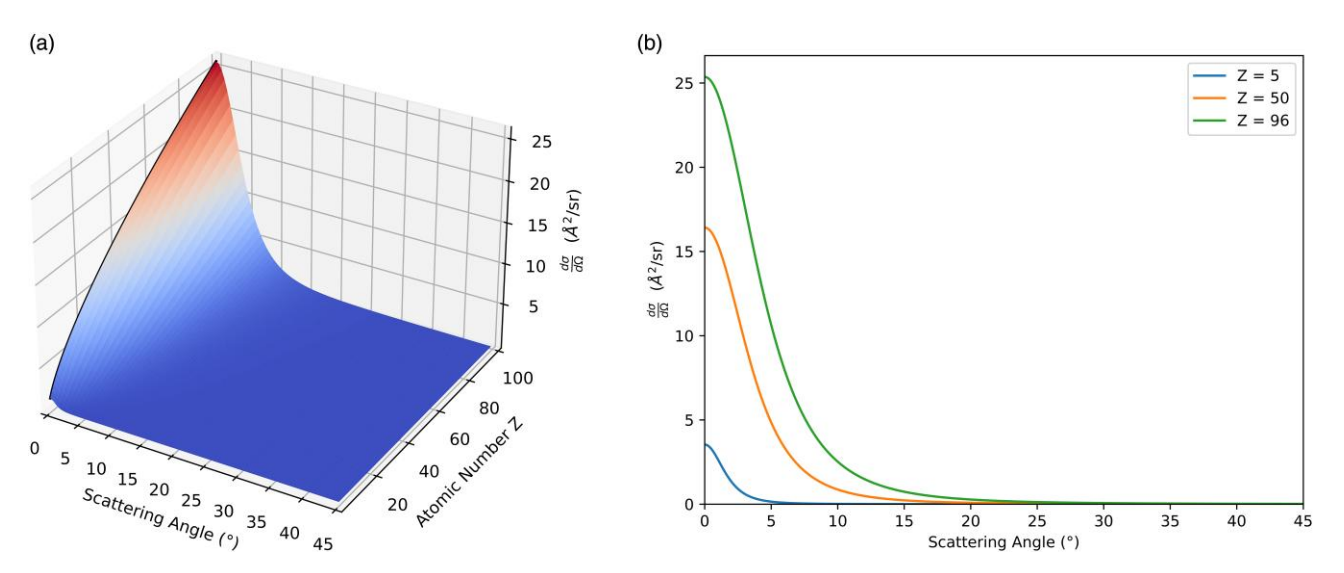


Fig. 10. Scattering probabilities as a function of atomic number Z and scattering angle θ (a) and for selected atomic numbers Z = 5, 50, and 96 (b). Both are plotted with E = 20 keV.

Table 1. Average Scattering Characteristics for Electrons Exiting Sample With Energies Greater than 500 eV in Monte Carlo Simulations.

Sample	Number of Backscattered e ⁻	Average Scattering Angle	Average Maximum Scattering Angle	Average Small Angle Scattering
Aluminum	15,669	12.35	83.93	9.62
Copper	30,092	19.82	93.50	15.38
Gold	45,680	18.92	121.29	13.06

The average small angle scattering is the average of all scattering angles without the maximum scattering angle included. 100,000 electrons accelerated to 15 keV were incident on each simulated material.

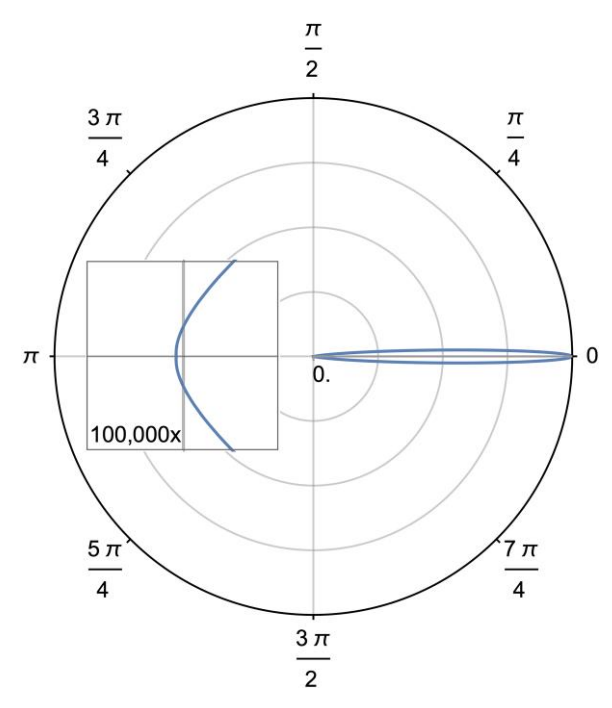


Fig. 11. Polar depiction of the full angular dependence of the differential cross section, normalized by the maximum at theta = 0, for Z = 29 at 20 keV. The inset, on a 100,000 times smaller scale, shows the relatively small number of complete (180 degrees) backscattering events.

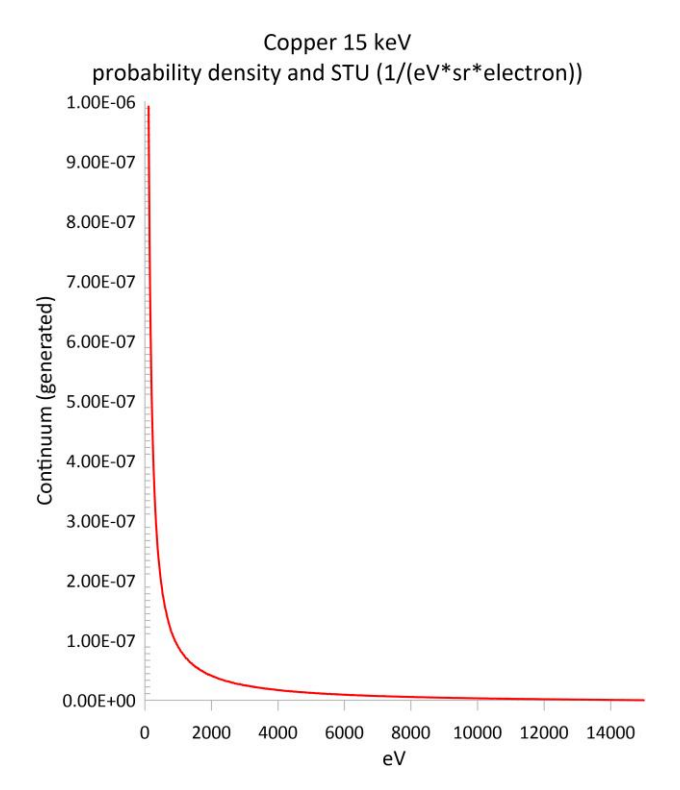


Fig. 12. Generated continuum radiation in copper at 15 keV. The vast majority of bremsstrahlung production is from low energy (small angle) electron scattering demonstrating the relatively large number of small energy scattering events producing continuum photons.

matrix correction, we are looking at an accuracy error of around 4% relative in such materials. In fact, we suspect this is one reason many analysts seem to require the use of so-called "matrix matched" standards for best accuracy. We believe that only through the use of a Yukawa Z fraction based analysis can we adequately handle these mass induced biases in our quantitative analyses.

Further, albeit indirect, evidence for this assertion is demonstrated in Figure 16, which shows WDS measurements of

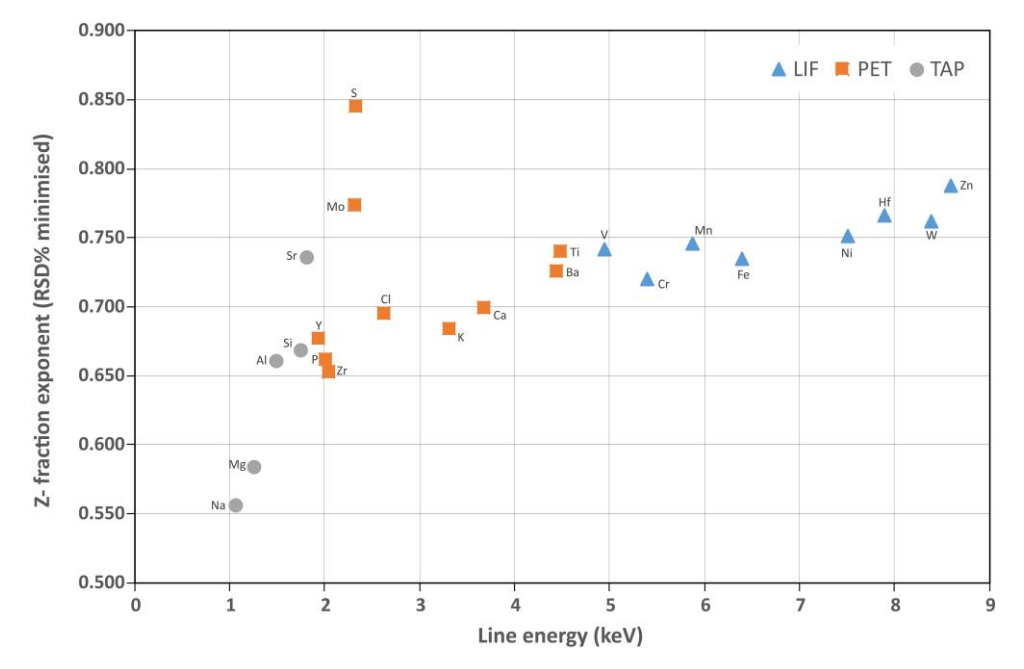


Fig. 13. Best fit Z fraction exponents for continuum measurements over a range of emission line energies for compounds that do not contain the emitting element using absorption corrected intensities. As expected, higher energy lines of higher Z elements show a best fit Z fraction exponent slightly greater than 2/3

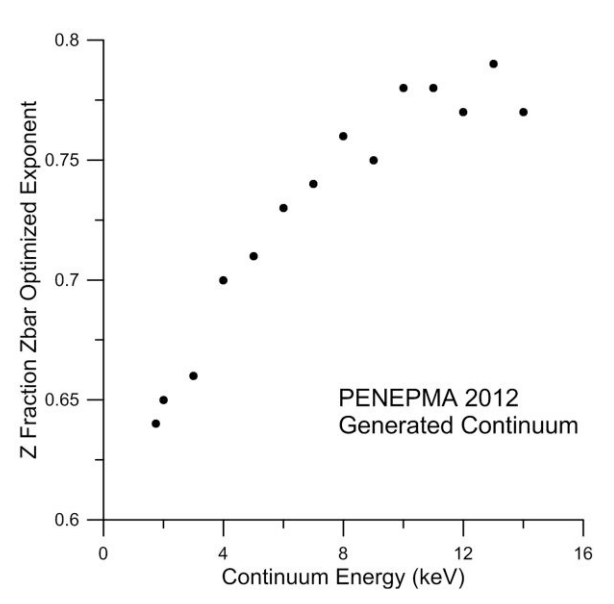


Fig. 14. Plot of optimized Z fraction exponents from PENEPMA 2012 Monte Carlo simulations of generated continuum intensities for a range of continuum emission energies. As previously shown by empirical measurements in Figure 13, at higher energies the optimum Z fraction exponent, for a range of pure elements and compounds, demonstrates a positive trend increasing from 2/3 to slightly higher values as expected.

characteristic emission lines for Ni K α , Cu K α , and Mo L α X-rays in pure metals. Both natural abundance material and enriched stable isotope material from the Oak Ridge Stable Isotope Repository were used in two sample splits. Fractional atomic mass numbers are averages for natural isotopic mixtures presented for comparison with masses for enriched isotopes. Each point represents an average of 10 measurements, shown relative to the average intensity measured for both natural and enriched isotopes; each error bar

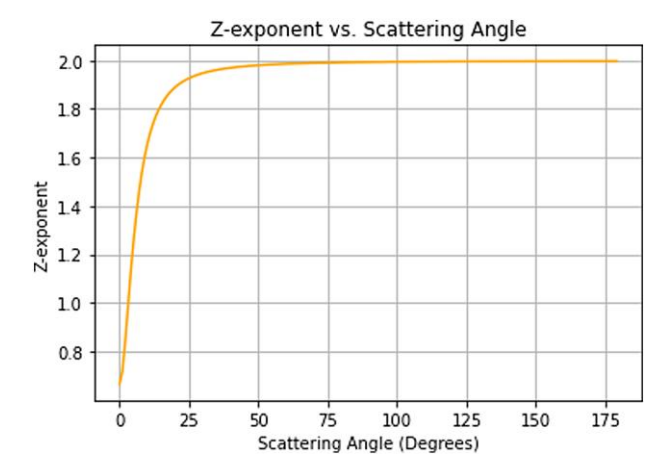


Fig. 15. Plotting average scattering angle as a function of the Z exponent, we see the highest probability is close to $Z^{2/3}$ for average scattering angles approaching zero, thus demonstrating that $Z^{\sim 2/3}$ is the dominant exponent as opposed to Z^2 . Details of this calculation are found in the Appendix.

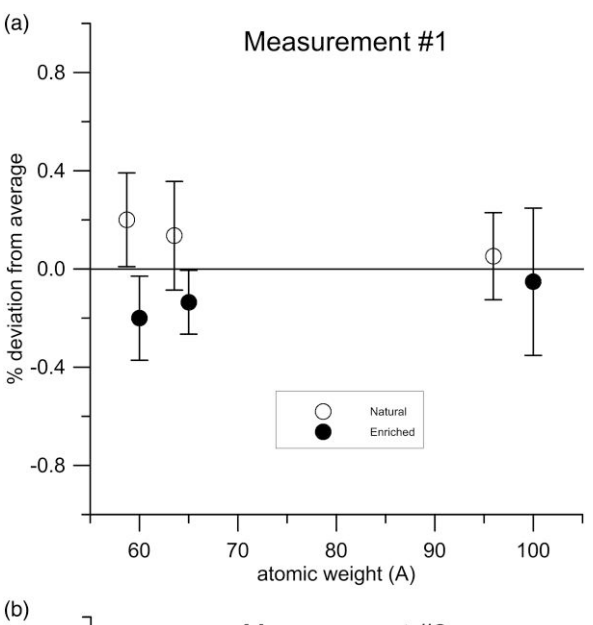
is one standard deviation. The complete analysis (Measurement #1) was repeated for verification on a second probe mount of a separate set of isotope pairs (Measurement #2). Conventional mass fraction averaging implies that the X-ray emission from ⁶⁰Ni, ⁶⁵Cu, and ¹⁰⁰Mo should be 1.7%, 2.3%, and 4% greater than from natural Ni, Cu, and Mo, respectively. Note that all the measurements fall within 0.25% of the respective average of each isotope pair, and that even the one-standard-deviation error bars are within 0.5% of the average. These observed deviations are far less than the differences expected under atomic mass based assumptions.

Some may argue that we currently successfully utilize mass fractions in our stopping power and absorption correction

Table 2. Comparison of Concentrations Expressed in Mass Fractions, $Z^{(1.0)}$ Fractions, and $Z^{(0.7)}$ Fractions Along With the Relative Differences for Each Element, and the Mass, $Z^{(1.0)}$ Fractions, and $Z^{(0.7)}$ Fractions for Several Compounds Showing a Range of A/Z Effects.

Compound	Element	Mass Fraction	Z Fraction $(Z^{1.0})$	Relative Difference (%)	Z Fraction $(Z^{0.7})$	Relative Difference (%)	Mass Zbar	Z Fraction (Z ^{1.0}) Zbar	Z Fraction (Z ^{0.7}) Zbar
MgO	Mg	0.6030	0.6000	-0.50	0.5705	-5.40	10.4121	10.4000	10.2819
	O	0.3970	0.4000	0.76	0.4295	8.20			
- 2	Ti	0.5995	0.5789	-3.43	0.5037	-15.97	16.3930	16.1053	15.0524
	O	0.4005	0.4211	5.13	0.4963	23.91			
GaAs	Ga	0.4820	0.4844	0.49	0.4890	1.46	32.0360	32.0313	32.0219
	As	0.5156	0.5156	-0.46	0.5110	-1.36			
ZrSiO ₄	Zr	0.4976	0.4651	-6.53	0.3602	-27.61	24.8439	23.8606	20.5637
	Si	0.1532	0.1628	6.25	0.1728	12.75			
	O	0.3491	0.3721	6.57	0.4670	33.77			
PbS	Pb	0.8660	0.8368	-3.38	0.7584	-12.42	73.1560	71.23	66.0557
	S	0.1340	0.1632	21.83	0.2416	80.28			

Note the large relative differences in results when comparing traditional mass fractions and mass fraction derived average Z values to Z Fraction derived values for compounds with disparate A/Z ratios.



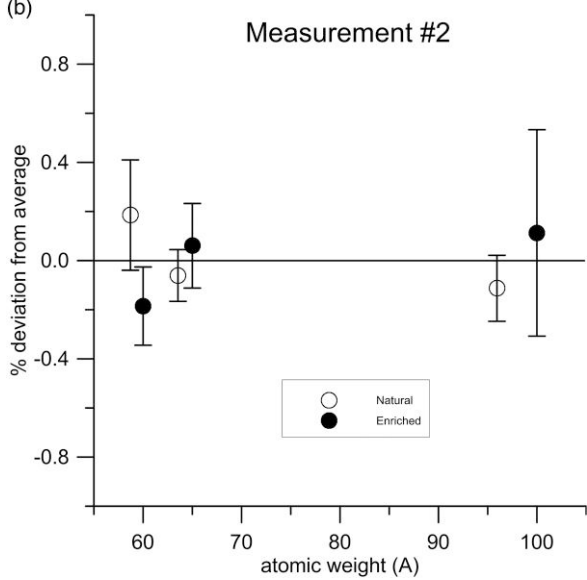


Fig. 16. EPMA measurements of characteristic emission lines in natural abundance and enriched stable isotopes from the Oak Ridge Stable Isotope Repository in nickel, copper, and molybdenum for two separate splits of the materials (**a**) and (**b**). There is up to an almost 5% relative difference in the average atomic weights for these material pairs. This weight differential is significantly greater than the precision of the measurements.

calculations, but this is only because we simultaneously utilize associated parameters which are already normalized to mass, i.e., mass thickness and mass absorption coefficients. Such mass based modeling is not utilized in purely physics based Monte Carlo approaches, as we have demonstrated in the PENEPMA 2012 simulations. It is worth considering what mass biased results we might obtain from measuring isotope enriched materials such as ²⁹Si in silicates, while utilizing a natural abundance standard, if we insist on expressing our results in mass fractions. Similarly, by utilizing Yukawa based Z fraction concentrations, we can also eliminate such mass bias effects in our analysis of normal isotopic abundance materials.

Conclusion

We argue that the traditional inclusion of mass in average Z calculations for microanalysis merely introduces a bias related to the A/Z ratio of the elements in compounds and suggest that, for improved accuracy in electron backscatter loss and continuum production modeling, only a Z dependent calculation be adopted for quantitative analysis. We have presented both experimental data as well as Monte Carlo simulations that both show excellent fits to predicted values when the Z fraction is raised to an exponent of approximately 0.7, and we provide a simple theoretical model for electron scattering from screened atomic potentials that predicts a similar Z fraction exponent of 2/3 that is consistent with an experimentally derived value.

Future work will attempt to provide a Yukawa Z fraction based matrix correction method for quantitative microanalysis in which a suitable table of atomic weights will only be utilized to convert our (standard) concentrations from mass fractions to Yukawa Z fractions, and subsequently to convert our matrix corrected (unknown) results using a similarly appropriate table of atomic weights for these unknowns, from (Yukawa) Z fractions to mass fractions for final reporting of the analysis results in traditional mass units.

Acknowledgments

The authors would like to thank two anonymous reviewers for their helpful comments and suggestions and also acknowledge Edward Vicenzi (The Smithsonian Institution) as an internal reviewer for this manuscript. His comments and suggestions were most helpful.

Financial Support

The current study has not received any funding from any organizations or institutions.

Conflict of Interest

John Donovan is the president of Probe Software which offers automation and analysis software for EPMA instruments.

References

Büchner AR (1973). Bestimmung der mittleren Ordnungszahl von Legierungen bei der quantitativen Mikrosondenanalyse. *Arch Eisenhüttenwesen* 44, 143–147. https://doi.org/10.1002/srin.197304509

Carron NJ (2006). An Introduction to the Passage of Energetic Particles Through Matter. Boca Raton, FL: CRC Press.

Danguy L & Quivy R (1956). Rétrodiffusion (backscattering) des électrons par les solutions et les alliages. *J Phys Rad* 17, 320. https://doi.org/10.1051/jphysrad:01956001704032000

Donovan JJ & Pingitore NE (2002). Compositional averaging of continuum intensities in multi-element compounds. *Microsc Microanal* 8, 429–436. https://doi.org/10.1017/S1431927602020160

Donovan JJ, Pingitore NE & Westphal A (2003). Compositional averaging of backscatter intensities in compounds microscopy & microanalysis. *Microsc Microanal* 9, 202–215. https://doi.org/10.1017/S1431927603030137

Egerton R (2011). Electron Energy Loss Spectroscopy in the Electron Microscope. New York, NY: Springer.

Everhart TE (1960). Simple theory concerning the reflection of electrons from solids. J Appl Phys 31, 1483–1490. https://doi.org/10.1063/1. 1735868

Giannozzi P, Andreussi O, Brumme T, Bunau O, Nardelli MB, Calandra M, Car R, Cavazzoni C, Ceresoli D, Cococcioni M, Colonna N, Carnimeo I, Dal Corso A, de Gironcoli S, Delugas P, DiStasio R A, Ferretti A, Floris A, Fratesi G, Fugallo G, Gebauer R, Gerstmann U, Giustino F, Gorni T, Jia J, Kawamura M, Ko H-Y, Kokalj A, Küçükbenli E, Lazzeri M, Marsili M, Marzari N, Mauri F, Nguyen N L, Nguyen H-V, Otero-de-la-Roza A, Paulatto L, Poncé S, Rocca D, Sabatini R, Santra B, Schlipf M, Seitsonen A P, Smogunov A, Timrov I, Thonhauser T, Umari P, Vast N, Wu X & Baroni S (2017). Advanced capabilities for materials modelling with quantum ESPRESSO. *J Phys Condens Matter* 29, 465901. https://doi.org/10.1088/1361-648X/aa8f79

Giannozzi P, Baroni S, Bonini N, Calandra M, Car R, Cavazzoni C, Ceresoli D, Chiarotti GL, Cococcioni M, Dabo I, Dal Corso A, de Gironcoli S, Fabris S, Fratesi G, Gebauer R, Gerstmann U, Gougoussis C, Kokalj A, Lazzeri M, Martin-Samos L, Marzari N, Mauri F, Mazzarello R, Paolini S, Pasquarello A, Paulatto L, Sbraccia C, Scandolo S, Sclauzero G, Seitsonen AP, Smogunov A, Umari P & Wentzcovitch RM (2009). QUANTUM ESPRESSO: A modular and open-source software project for quantum simulations of materials. *J Phys Condens Matter* 21, 395502. https://doi.org/10.1088/0953-8984/21/39/395502

Goldstein JI, Newbury DE, Echlin P, Joy DC, RomigJr AD, Lyman CE, Fiori C & Lifshin E (1992). Scanning Electron Microscopy and X-Ray Microanalysis. A Text for Biologists, Materials Scientists, and Geologists, Xviii+, pp. 820. New York, London: Plenum Press.

Griffiths DJ & Schroeter DF (2020). Chapter 11—Scattering. In Introduction to Quantum Mechanics, Second Edition, pp. 394–419. Cambridge, United Kingdom: Cambridge University Press.

Herrmann R & Reimer L (1984). Backscattering coefficient of multicomponent specimens. *Scanning* 6, 20–29. https://doi.org/10.1002/ sca.4950060203

Howell PGT, Davy KMW & Boyde A (1998). Mean atomic number and backscattered electron coefficient calculations for some materials with low mean atomic number. *Scanning* 20, 35–40. https://doi. org/10.1002/sca.1998.4950200105 Joyet G, Trumpy-Eggenberger C & Mauderli W (1953). *The Dosage of Gamma Radiation at Very High Energies*. Baden, Switzerland: The Brown Boveri Betatron, Brown Boveri and Co. Ltd.

Kittel C (2004). Introduction to Solid State Physics, 8th edition. Hoboken, NI: Wiley.

Llovet X & Salvat F (2017). PENEPMA: A Monte Carlo program for the simulation of X-ray emission in electron probe microanalysis. *Microsc Microanal* 23, 634–646. https://doi.org/10.1017/ S1431927617000526

Moy A, von der Handt A, Fournelle J, Nachlas W & Donovan J (2021). Universal Mean Atomic Number curves for EPMA calculated by Monte Carlo simulations. *Microsc Microanal* 27(S1), 1098–1101. https://doi.org/10.1017/S143192762100413X

Packwood RH & Brown JD (1981). A Gaussian expression to describe φ (pz) curves for quantitative electron probe microanalysis. *X-ray Spectrom* 10(3), 138–146. https://doi.org/10.1002/xrs. 1300100311

Perdew JP, Burke K & Ernzerhof M (1996). Generalized gradient approximation made simple. *Phys Rev Lett* 77, 3865–3868. https://doi.org/10.1103/PhysRevLett.77.3865

Reimer K (1998). Scanning Electron Microscopy. New York, US: Springer.

Saldick J & Allen AO (1954). The oxidation of ferrous sulphate in acid solution by high energy cathode rays. *J Chem Phys* **22**, 438–442. https://doi.org/10.1063/1.1740087

Yukawa H (1935). On the interaction of elementary particles. I. *Proc Phys Math Soc Jpn 3rd Ser* 17, 48–57. https://doi.org/10.1143/PTPS.1.1

Appendix: Variability of Z exponent with scattering angle θ

The result of "The Differential Scattering Cross Section of the Yukawa Potential" is the function

$$\frac{d\sigma}{d\Omega} = |f(\theta)|^2 = 4a_0^2 \gamma^2 Z^{\frac{2}{3}} \left[1 + \left(2ka_0 Z^{-\frac{1}{3}} \right)^2 \sin^2 \left(\frac{\theta}{2} \right) \right]^{-2}.$$

We observe $\frac{d\sigma}{d\Omega}$ is a rational function of Z, i.e., $\frac{d\sigma}{d\Omega} = \frac{d\sigma}{d\Omega}(\theta, Z)$, that simplifies into a true polynomial when evaluated at $\theta = 0^{\circ}$. However, for any θ , we can validly fit the differential cross section to $y = \alpha Z^{\beta}$, where α and β are the fitting parameters. Figure 15 plots our Z exponent, the parameter β , as a function of θ .

More rigorously, we can calculate the numerical value of the different coefficients in the previous equation. a_0 is the Bohr

radius of
$$5.29 \times 10^{-11}$$
 m and $k = \frac{\gamma m_e c}{\hbar} \sqrt{1 - \left(\frac{m_e c^2}{m_e c^2 + E}\right)^2}$ is the momentum of the electron where m_e is the mass of the electron, \hbar is the reduced Planck constant, and E is the electron energy in keV. For a beam energy of 20 keV, typical for EPMA, we have $k = 7.32 \times 10^{11}$ m⁻¹.

The above equation can be rewritten as

$$\frac{d\sigma}{d\Omega}(\theta) = 4a_0^2 \gamma^2 * \frac{Z^2}{\left[Z^{2/3} + 4a_0^2 k^2 \sin^2(\frac{\theta}{2})\right]^2}$$

which, once expanded, is of the form

$$\frac{d\sigma}{d\Omega}(\theta) = A * \frac{Z^2}{Z^{4/3} + B * Z^{2/3} + C}$$

where $A = 4a_0^2 \gamma^2$, $B = 8a_0^2 k^2 \sin^2(\frac{\theta}{2})$, and $C = 16a_0^4 k^4 \sin^4(\frac{\theta}{2})$. Choosing $\theta = 180^\circ$ to maximize B and C, and keeping E = 20 keV, we have A = 1.21 m², $B = 1.20 \times 10^4$, and $C = 3.59 \times 10^7$. We consider elements of atomic number between 1 and 99, so $Z^{2/3} \in [1^{2/3}, 99^{2/3}] = [1, 21.40]$ and $Z^{4/3} \in [1, 457.98]$.

These values are too small to prevent C from being the dominant term, leaving the differential cross section to be proportional to Z^2 .

To extend the domain of validity of this reasoning, we assume EPMA analyses use electron beam energies ranging from 5 keV to 40 keV. A has a very light energy dependence in this regime, changing from 1.14 to 1.30 with this increase in acceleration voltage. Otherwise, at 5 keV and Z = 99, $BZ^{2/3} = 6.32 \times 10^4$ and $C = 2.18 \times 10^6$. At 40 keV and

Z = 99, $BZ^{2/3} = 5.23 \times 10^5$ and $C = 1.49 \times 10^8$. And, while we've ignored the angular dependence of B and C in this analysis, $\sin^4(\frac{\theta}{2})$ is the same order of magnitude as $\sin^2(\frac{\theta}{2})$ for $36.87^\circ < \theta \le 180^\circ$. Consequently, at large scattering angles for all beam energies used in EPMA, the differential cross section can be approximated by

$$\frac{d\sigma}{d\Omega}(\theta > 37^{\circ}) \approx \frac{A}{C}Z^{2}$$
.